Potential and string breaking of doubly heavy baryon at finite temperature and chemical potential

Bo Yu, Xi Guo, Xun Chen,* and Xiao-Hua Li†

School of Nuclear Science and Technology, University of South China, Hengyang 421001, China

(Received 31 May 2023; accepted 25 July 2023; published 11 September 2023)

Using gauge/gravity duality, we first study the string breaking and melting of doubly heavy baryon at a finite chemical potential and temperature in this paper. The decay mode $QQq \to Qqq + Q\bar{q}$ is investigated with the presence of temperature and chemical potential in this paper. With the increase of temperature and chemical potential, string breaking takes place at a smaller potential energy, and the string-breaking distance will increase slightly. It is also found that the QQq melts at a small separate distance with the increase of temperature and chemical potential. Then, we compare the screening distance of QQq with $Q\bar{Q}$ under the same conditions. Finally, we draw the melting diagram of QQq and $Q\bar{Q}$ in the $T-\mu$ plane.

DOI: 10.1103/PhysRevD.108.066007

I. INTRODUCTION

The interquark potential is one of the crucial factors in determining the formation of baryonic bound states, and investigating the potential can facilitate a further understanding of the structure of baryons and the dynamical mechanisms of QCD. Due to computational limitations, predicting the properties of hadrons remains a daunting challenge in QCD. Research on heavy quarks and static test charges is valuable for probing the confinement properties of QCD, as they share similar characteristics.

Lattice QCD remains the most reliable theoretical method for studying nonperturbative physics in QCD [1–8]. Despite QCD at finite chemical potential can be formulated on the lattice [9]; however, standard Monte Carlo techniques cannot be used at $\mu \neq 0$. Some methods have been proposed to address this issue [10,11], but the study of lattice QCD under finite temperature and chemical potential is still challenged due to the presence of the fermion sign problem. As we know, high temperatures, densities, and other extreme conditions are produced in relativistic heavy-ion collision experiments. It is essential to compare various nonperturbative methods to obtain a more comprehensive theoretical understanding of the nonperturbative physics in QCD [12–16].

The success of the Cornell model in describing quarkonium spectroscopy has had a profound impact on the further development of potential energy models and other approaches to nonrelativistic QCD [17–19]. As a crucial ingredient in our understanding of strong interactions, the study of quark-antiquark potential is already sufficient through the study of a deformed AdS_5 model and the Einstein-Maxwell-Dilation model, etc., [20–46].

The applicability of perturbative methods to high-energy processes and phenomena is limited by the large coupling of strong interactions in the low-energy region. The development of the holographic principle and the AdS/CFT correspondence [47] provides us with a new approach to study strongly coupled nuclear matter in the low-energy region and at energy scales close to the deconfined phase transition temperature.

A holographic model developed from string theory has been proposed, which employs the Nambu-Goto action of strings at zero and finite temperature in higher-dimensional spacetime to calculate the Coulomb potential and screening effect between quarks and antiquarks [48–50]. These researches provide a new approach for researching meson interactions. A holographic baryon is considered to be a D-brane that wraps the inner subspace of the background spacetime, with a string connecting it and extending to the boundary [46,51]. Furthermore, Andreev proposed a string theoretical structure for the QQq system based on previous studies on the heavy quark potential in [52–55], enabling us to investigate its ground state.

The basic task of this paper is to extend effective string models of holographic QCD to finite temperatures and chemical potentials. In this model, two heavy quarks are connected by string to the baryon vertex which is a five-brane; the light quark is a tachyon field coupled to the world-sheet boundary. The rest of the paper is organized as follows: Different configurations are discussed at finite temperature and chemical potential in Sec. II. Then, we numerically solved these configurations, and the potential

*chenxunhep@qq.com
†lixiaohuaphysics@126.com

of QQq is discussed in Sec. III. Finally, the main results of this paper are summarized in Sec. IV.

II. THE SETUP

We start with a general metric ansatz [53,56],

$$ds^2 = e^{sr^2}\frac{R^2}{r^2}(f(r)dt^2 + d\vec{x}^2 + f^{-1}(r)dr^2) + e^{-sr^2}g^{(5)}_{ab}d\omega^a d\omega^b. \quad (1)$$

This model parametrized by s is a one-parameter deformation of Euclidean AdS_5 space and a five-dimensional compact space (sphere) $\mathbf{X}$ whose coordinates are ω^a. The radius R is a constant, and $f(r)$ is a blacken factor of the black hole. The Hawking temperature of the black hole is defined as

$$T = \frac{1}{4\pi}\left|\frac{df}{dr}\right|_{r=r_h} = \frac{1}{\pi r_h}\left(1-\frac{1}{2}Q^2\right). \quad (2)$$

Here, with $Q = q{r_h}^2$ and $0 \le Q \le \sqrt{2}$, r_h is the position of the black hole horizon. When r is small, the behavior of the bulk gauge field is $A_0(r) = \mu - \eta r^2$ with $\eta = \kappa q$, where κ is a dimensionless parameter, and q is the charge of the black hole. Together with the boundary conditions $A_0(r_h) = 0$ and $A_0(0) = \mu$, we can acquire the relation between the baryon chemical potential μ and black charge q, which can be expressed as

$$\mu = q\kappa r_h^2 = \kappa\frac{Q}{r_h}. \quad (3)$$

Following Refs. [14,53,56], we fix the parameter κ to 1. Furthermore, we have following three relationships:

$$f(r) = 1 - \left(\frac{1}{r_h^4} + \frac{\mu^2}{r_h^2}\right)r^4 + \frac{\mu^2}{r_h^4}r^6,$$
$$T = \frac{1}{\pi r_h}\left(1-\frac{1}{2}\mu^2 r_h^2\right),$$
$$A_0(r) = \mu - \mu\frac{r^2}{r_h^2}. \quad (4)$$

Noticeably, $A_0(r)$ is a quantity that is dependent on μ as well as the horizon r_h.

As is similarly discussed in Refs. [19,56], the string structure contains three parts: three quarks, the baryon vertex V, and the strings among them. There are three basic ingredients to construct the string configuration.

Firstly, the Nambu-Goto action of a string is expressed as the following expression:

$$S_{\mathrm{NG}} = \frac{1}{2\pi\alpha'}\int_0^1 d\sigma\int_0^T d\tau\sqrt{\gamma}, \quad (5)$$

where γ is an induced metric on the string world sheet.

Secondly, the baryon vertex is considered to be a five-brane according to the AdS/CFT dictionary. Since we are interested in a static quark potential, we choose a static gauge $\xi^0 = t$ and $\xi^a = \theta^a$ with θ^a coordinates on $\mathbf{X}$. The action of the baryon vertex is given by

$$S_{\mathrm{vert}} = \tau_v\int dt\frac{e^{-2sr^2}}{r}\sqrt{f(r)}, \quad (6)$$

where τ_v is a dimensionless parameter defined by $\tau_v = \mathcal{T}_5 R\,\mathrm{vol}(\mathbf{X})$, and $\mathrm{vol}(\mathbf{X})$ is a volume of $\mathbf{X}$ [14,52,56].

Thirdly, the ingredient of the light quark at the string endpoint is a sigma-model action in a tachyon background. As illustrated in Ref. [56], the action S_q could be written as

$$S_{\mathrm{q}} = \mathrm{m}\int dt\frac{e^{\frac{s}{2}r^2}}{r}\sqrt{f(r)}, \quad (7)$$

where $\mathrm{m} = RT_0$. This is the action of a point particle of mass T_0 at rest. The model parameters need to be fixed as follows: $\mathbf{g} = \frac{R^2}{2\pi\alpha'}$, $k = \frac{\tau_v}{3\mathbf{g}}$, and $n = \frac{m}{\mathbf{g}}$.

Finally, when the string endpoints with attached quarks couple to a background gauge field [16,53], the world sheet action includes boundary terms that could be given by

$$S_{\mathrm{A}} = \mp\frac{1}{3}\int dt A_0. \quad (8)$$

The minus and plus signs correspond to a quark and an antiquark.

As separate distance L grows, there are three configurations in the model.

A. Small L

The first configuration is plotted in Fig. 1. The total action is the sum of the Nambu-Goto actions, the action for the vertex, light quark, and boundary terms,

$$S = \sum_{i=1}^{3} S^{(i)}_{\mathrm{NG}} + S_{\mathrm{vert}} + S_{\mathrm{q}} + 2S_{\mathrm{A}}|_{r=r_Q} + S_{\mathrm{A}}|_{r=r_q}. \quad (9)$$

If we choose the static gauge $\xi^1 = t$ and $\xi^2 = r$, then the boundary conditions for $x(r)$ are

$$x^{(1)}(0) = -\frac{L}{2}, \qquad x^{(2)}(0) = \frac{L}{2}, \qquad x^{(i)}(r_v) = x^{(3)}(r_q) = 0. \quad (10)$$

The total action can be written as

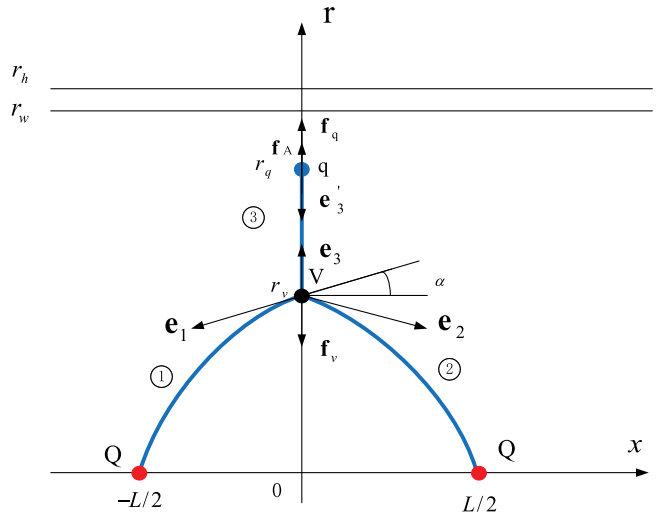

FIG. 1. The first static string configuration at a small heavy quark separation. The heavy quarks Q are placed at the x axis. The light quark and baryon vertex V are on the r axis at $r = r_q$ and $r = r_v$, respectively. The quarks and baryon vertex are connected by blue strings. The force exerted on the vertex and light quark are depicted by the black arrows. r_h is the position of the black-hole horizon. r_w is the position of the dynamic wall.

$$S = \mathbf{g}T\left(2\int_0^{r_v}\frac{dr}{r^2}\mathrm{e}^{sr^2}\sqrt{1+f(r)(\partial_r x)^2} + \int_{r_v}^{r_q}\frac{dr}{r^2}\mathrm{e}^{sr^2}\sqrt{1+f(r)(\partial_r x)^2} + 3\mathrm{k}\frac{\mathrm{e}^{-2sr_v^2}}{r_v}\sqrt{f(r_v)} + \mathrm{n}\frac{\mathrm{e}^{\frac{1}{2}sr_q^2}}{r_q}\sqrt{f(r_q)}\right) - \frac{1}{3}A_0(r_q) - \frac{2}{3}A_0(0), \tag{11}$$

where $\partial_r x = \frac{\partial x}{\partial r}$ and $T = \int_0^T dt$. We consider the first term in Eq. (11) which corresponds to string ① and string ②. Due to symmetry, the result of the string ② is exactly the same as that of the string ①. The equation of motion for $x(r)$ can be obtained from the Euler-Lagrange equation. It reduces to

$$\mathcal{I} = \frac{w(r)f(r)\partial_r x}{\sqrt{1+f(r)(\partial_r x)^2}}, \qquad w(r) = \frac{\mathrm{e}^{sr^2}}{r^2}. \tag{12}$$

$\mathcal{I}$ is a constant. At r_v, we have $\partial_r x|_{r=r_v} = \cot\alpha$ with $\alpha > 0$, and

$$\mathcal{I} = \frac{w(r_v)f(r_v)\cot\alpha}{\sqrt{1+f(r)\cot^2\alpha}}. \tag{13}$$

$\partial_r x$ can be solved as

$$\partial_r x = \sqrt{\frac{\omega(r_v)^2 f(r_v)^2}{(f(r_v)+\tan^2\alpha)\omega(r)^2 f(r)^2 - f(r)w(r_v)^2 f(r_v)^2}}. \tag{14}$$

By virtue of Eq. (14), the integral over $[0, r_v]$ of dr is

$$L = 2\int_0^{r_v}\frac{dx}{dr}dr. \tag{15}$$

The regularized energy after subtracting the divergent term $\mathbf{g}\int_0^\infty dr\frac{1}{r^2}$ from the first term of Eq. (11) can be expressed as

$$E_1 = \frac{S}{T} = \mathbf{g}\int_0^{r_v}\left(\frac{1}{r^2}\mathrm{e}^{sr^2}\sqrt{1+f(r)(\partial_r x)^2} - \frac{1}{r^2}\right)dr - \frac{\mathbf{g}}{r_v} + c. \tag{16}$$

Here c is a normalization constant. As string ③ is straight stretched between the vertex and light quark from Eq. (11), the energy of which could be calculated as

$$E_2 = \mathbf{g}\int_{r_v}^{r_q}\frac{\mathrm{e}^{sr^2}}{r^2}dr. \tag{17}$$

To this end, the energy could be written as

$$E_{\mathrm{QQq}} = \mathbf{g}\left(2\int_0^{r_v}\left(\frac{1}{r^2}\mathrm{e}^{sr^2}\sqrt{1+f(r)(\partial_r x)^2} - \frac{1}{r^2}\right)dr - \frac{2}{r_v} + \mathrm{n}\frac{\mathrm{e}^{\frac{1}{2}sr_q^2}}{r_q} + 3\mathrm{k}\frac{\mathrm{e}^{-2sr_v^2}}{r_v}\sqrt{f(r_v)}\right) - \frac{1}{3}A_0(r_q) - \frac{2}{3}A_0(0) + 2c. \tag{18}$$

It is easy to find that the potential energy is a function of r_v,r_h and angle α. As discussed before, μ, T, and r_h have a relationship as Eq. (4). Therefore, one can study the potential of QQq in a model associated with the temperature and chemical potential. The main point becomes to determine r_q (the position of the light quark) and angle α. Using the force balance equation with respect to r_q and r_v, we can achieve this goal.

Firstly, the force balance equation at r_q is

$$f_q + e'_3 + f_A = 0. \tag{19}$$

By varying the action for r_q, it is found that $f_q = (0, -\mathbf{g}n\partial_{r_q}(\frac{\mathrm{e}^{\frac{1}{2}sr_q^2}}{r_q}\sqrt{f(r_q)}))$, $f_A = \frac{\partial A_0(r)}{\partial r}$, and the string tension $\mathbf{e}'_3 = \mathbf{g}w(r_q)(0,-1)$. Therefore, the balance equation becomes

$$2{r_q}^2\sqrt{f(r_q)}A'_0(r_q) - 3\mathbf{g}ne^{\frac{{r_q}^2 s}{2}}(r_q f'(r_q) + 2f(r_q)({r_q}^2 s - 1)) - 6g\sqrt{f(r_q)}e^{{r_q}^2 s} = 0. \tag{20}$$

With a suitable T and μ fixed, r_h can be solved through Eq. (4). By solving Eq. (20), we find that r_q only depends

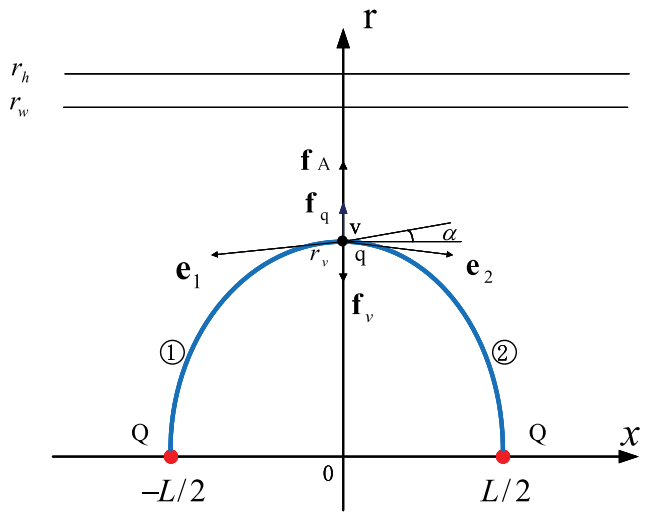

FIG. 2. The second static string configuration at an intermediate heavy quark separation. The heavy quarks Q are placed at the x axis. The light quark and baryon vertex V are on the r axis at the same point. The quarks and baryon vertex are connected by blue strings. The force exerted on the vertex and light quark are depicted by the black arrows. r_h is the position of the black-hole horizon. r_w is the position of the dynamic wall.

on r_h. Hereafter, turning to the angle α, the force balance equation on the vertex can be expressed as

$$\mathbf{e}_1 + \mathbf{e}_2 + \mathbf{e}_3 + \mathbf{f}_v = 0. \tag{21}$$

We adopt the same manner as [15], and we get such a result; the force on the vertex is $\mathbf{f}_v = (0, -3\mathbf{g}k\partial_{r_v}(\frac{e^{-2sr_v^2}}{r_v}\sqrt{f(r_v)}))$, and string tensions are $\mathbf{e}_1 = \mathbf{g}w(r_v)(-\frac{f(r_v)}{\sqrt{\tan^2\alpha + f(r_v)}}, -\frac{1}{\sqrt{f(r_v)\cot^2\alpha+1}})$, $\mathbf{e}_2 = \mathbf{g}w(r_v)(\frac{f(r_v)}{\sqrt{\tan^2\alpha+f(r_v)}}, -\frac{1}{\sqrt{f(r_v)\cot^2\alpha+1}})$, $\mathbf{e}_3 = \mathbf{g}w(r_v)(0,1)$. The nontrivial component of the force balance equation is

$$\frac{3\mathbf{g}ke^{-2r_v{}^2s}(f(r_v)(8r_v{}^2s+2) - r_v f'(r_v))}{\sqrt{f(r_v)}} + 2\mathbf{g}e^{r_v{}^2s}\left(1 - \frac{2}{\sqrt{\cot^2\alpha f(r_v)+1}}\right) = 0. \tag{22}$$

The Eq. (22) provides us with a relationship between r_v and α. Then, we can numerically solve the energy E and separation distance L.

B. Intermediate L

In this configuration, the light quark coincides with the baryon vertex, and there are no strings between them. The angle α will gradually decrease to zero as the separation distance L increases. Thus, the total action of the configuration plotted in Fig. 2 can be expressed as

$$S = \sum_{i=1}^{2} S_{\mathrm{NG}}^{(i)} + S_{\mathrm{vert}} + S_{\mathrm{q}} + 2S_{\mathrm{A}}|_{r=r_Q} + S_{\mathrm{A}}|_{r=r_q}. \tag{23}$$

The static gauge is set in the same way as before. Thus, the total energy of the configuration is

$$E_{\mathrm{QQq}} = \mathbf{g}\left(2\int_0^{r_v}\left(\frac{1}{r^2}e^{\mathbf{s}r^2}\sqrt{1+f(r)(\partial_r x)^2} - \frac{1}{r^2}\right)dr - \frac{2}{r_v} + \mathrm{n}\frac{e^{\frac{1}{2}sr_v^2}}{r_v} + 3\mathrm{k}\frac{e^{-2sr_v^2}}{r_v}\sqrt{f(r_v)}\right) - \frac{1}{3}A_0(r_q) - \frac{2}{3}A_0(0) + 2c. \tag{24}$$

The only difference between the above equation with Eq. (18) is that r_q is replaced by r_v. Similarly, at r_q (or r_v), we have

$$\mathbf{e}_1 + \mathbf{e}_2 + \mathbf{f}_v + \mathbf{f}_q + \mathbf{f}_A = 0. \tag{25}$$

Each force could be given by

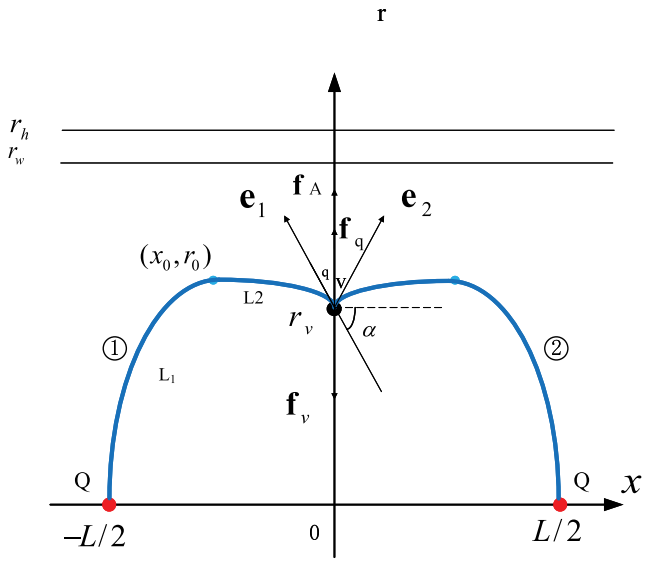

FIG. 3. The third static string configuration at a large heavy quark separation as the "U-shape" string transforms to an "M-shape" string. The heavy quarks Q are placed at the x axis. The light quark and baryon vertex V are on the r axis at $r = r_q = r_v$. The quarks and baryon vertex are connected by blue strings. The force exerted on the vertex and light quark are depicted by the black arrows. r_h is the position of the black-hole horizon. r_w is the position of the dynamic wall.

$$\mathbf{f}_q = \left(0, -n\mathbf{g}\partial_{r_v}\left(\frac{e^{\frac{1}{2}sr_v^2}}{r_v}\sqrt{f(r_v)}\right)\right),$$

$$\mathbf{f}_v = \left(0, -3\mathbf{g}k\partial_{r_v}\left(\frac{e^{-2sr_v^2}}{r_v}\sqrt{f(r_v)}\right)\right),$$

$$\mathbf{e}_1 = \mathbf{g}w(r_v)\left(-\frac{f(r_v)}{\sqrt{\tan^2\alpha + f(r_v)}}, -\frac{1}{\sqrt{f(r_v)\cot^2\alpha + 1}}\right),$$

$$\mathbf{e}_2 = \mathbf{g}w(r_v)\left(\frac{f(r_v)}{\sqrt{\tan^2\alpha + f(r_v)}}, -\frac{1}{\sqrt{f(r_v)\cot^2\alpha + 1}}\right),$$

$$\mathbf{f}_A = \frac{\partial A_0(r)}{\partial r}.$$

The force balance equation can be rearranged as

$$\frac{2r_v{}^2 e^{2r_v{}^2 s}A_0'(r_v)}{3\mathbf{g}} + \frac{3k(f(r_v)(8r_v{}^2 s + 2) - r_v f'(r_v))}{\sqrt{f(r_v)}} - \frac{ne^{\frac{5r_v{}^2 s}{2}}(r_v f'(r_v) + 2f(r_v)(r_v{}^2 s - 1))}{\sqrt{f(r_v)}} - \frac{4e^{3r_v{}^2 s}}{\sqrt{\cot\alpha^2 f(r_v) + 1}} = 0. \tag{26}$$

C. Large L

In this section, with the increase of r_v, the U-shape string develops to an M shape as in Fig. 3. To simplify the calculation, we choose another static gauge $\xi^1 = t$ and $\xi^2 = x$; the boundary conditions are

$$r^{(1)}(-L/2) = r^{(2)}(L/2) = 0, \qquad r^{(i)}(0) = r_v. \tag{27}$$

The total action becomes

$$S = \mathbf{g}T\left(\int_{-L/2}^{0} dx w(r)\sqrt{f(r) + (\partial_x r)^2} + \int_0^{L/2} dx w(r)\sqrt{f(r) + (\partial_x r)^2} + 3\mathrm{k}\frac{e^{-2sr_v^2}}{r_v}\sqrt{f(r_v)} + \mathrm{n}\frac{e^{\frac{1}{2}sr_v^2}}{r_v}\sqrt{f(r_v)}\right) - \frac{1}{3}A_0(r_v) - \frac{2}{3}A_0(0). \tag{28}$$

The action of the string could be given by the first two terms of Eq. (28). From the force balance equation at the baryon vertex, angle α can be similarly calculated in this configuration. In addition, we can use the first integral at points r_0 and r_v to obtain the relationship among r_0, r_v, and α,

$$\frac{w(r)f(r)}{\sqrt{f(r) + (\partial_x r)^2}} = w(r_0)\sqrt{f(r_0)},$$
$$\frac{w(r_v)f(r_v)}{\sqrt{f(r_v) + \tan\alpha^2}} = w(r_0)\sqrt{f(r_0)}. \tag{29}$$

After a short calculation, the solution for $\partial_x r$ can be written as

$$\partial_x r = \sqrt{\frac{w(r)^2 f(r)^2 f(r_0) - f(r)w(r_0)^2 f(r_0)^2}{w(r_0)^2 f(r_0)^2}}. \tag{30}$$

The separate distance consists of two parts separated by the turning point (x_0, r_0),

$$L = 2(L_1 + L_2) = 2\left(\int_0^{r_0}\frac{dx}{dr}dr + \int_{r_v}^{r_0}\frac{dx}{dr}dr\right) = 2\left(\int_0^{r_0}\sqrt{\frac{w(r_0)^2 f(r_0)^2}{w(r)^2 f(r)^2 f(r_0) - f(r)w(r_0)^2 f(r_0)^2}}dr + \int_{r_v}^{r_0}\sqrt{\frac{w(r_0)^2 f(r_0)^2}{w(r)^2 f(r)^2 f(r_0) - f(r)w(r_0)^2 f(r_0)^2}}dr\right). \tag{31}$$

Subtracting the divergent terms, the renormalized energy of string ① is

$$E=\mathbf{g}\int_{r_v}^{r_0}\left(w(r)\sqrt{\frac{w(r)^2f(r)^2f(r_0)}{w(r)^2f(r)^2f(r_0)-f(r)w(r_0)^2f(r_0)^2}}\right)dr+\mathbf{g}\int_0^{r_0}\left(w(r)\sqrt{\frac{w(r)^2f(r)^2f(r_0)}{w(r)^2f(r)^2f(r_0)-f(r)w(r_0)^2f(r_0)^2}}-\frac{1}{r^2}\right)dr$$
$$-\frac{\mathbf{g}}{r_v}+2c. \tag{32}$$

Since string ① and string ② are completely symmetric, the calculation method is the same, whereupon the total energy of the final configuration can be written as

$$E_{\mathrm{QQq}}=\mathbf{g}\left(2\int_{r_v}^{r_0}w(r)\sqrt{\frac{w(r)^2f(r)^2f(r_0)}{w(r)^2f(r)^2f(r_0)-f(r)w(r_0)^2f(r_0)^2}}dr\right.$$
$$\left.+2\int_0^{r_0}\left(w(r)\sqrt{\frac{w(r)^2f(r)^2f(r_0)}{w(r)^2f(r)^2f(r_0)-f(r)w(r_0)^2f(r_0)^2}}-\frac{1}{r^2}\right)dr-\frac{1}{r_0}+3\mathrm{k}\frac{\mathrm{e}^{-2\mathrm{s}r_v^2}}{r_v}\sqrt{f(r_v)}+\mathrm{n}\frac{\mathrm{e}^{\frac{1}{2}\mathrm{s}r_v^2}}{r_v}\sqrt{f(r_v)}\right)+2c. \tag{33}$$

Now that all the variables in the integral have been represented by r_v; we can numerically calculate the results of L and E_{QQq}.

III. NUMERICAL RESULT AND DISCUSSION

The string-breaking behavior can be judged from the total potential energy. Besides, the system will melt when T and μ become large enough. During the process of string melting, we compare the potential energies of doubly flavor baryons to those of quark-antiquark pairs at fixed temperature and chemical potential, respectively. String melting can be judged from the $L-r_v$ diagram. Within the margin of numerical error, we draw a $T-\mu$ melting diagram.

To approach the lattice result at vanishing temperature and chemical potential, all the parameters are fixed at vanishing temperature and chemical potential as follows: $s=0.42\ \mathrm{GeV}^2$, $\mathbf{g}=0.176$, $n=3.057$, and $c=0.623\ \mathrm{GeV}$ [19].

A. The numerical analysis of three configurations

According to the previous calculation procedure, the diagram of $L-r_v$ ($\mu=0.1$ GeV, $T=0.1$ GeV) and $E-L$ before string melting can be shown in Figs. 4 and 5. In Fig. 4, it is shown that the separate distance will increase with the increase of r_v. The presence of temperature and chemical potential will cause that the separate distance will tend to infinite at large r_v. In Fig. 5, we plot the potential energy of the quark-antiquark pair with a dot-dashed line

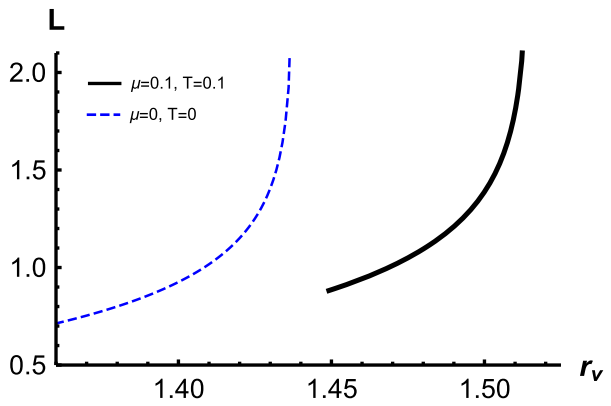

FIG. 4. At large separate distances, L as a function of r_v. The solid black and dashed blue lines correspond to the variations of L as a function of r_v for QQq at $\mu=0.1$ GeV, $T=0.1$ GeV, and $\mu=0$ GeV, $T=0$ GeV, respectively. The unit of L is fm; r_v is GeV^{-1}.

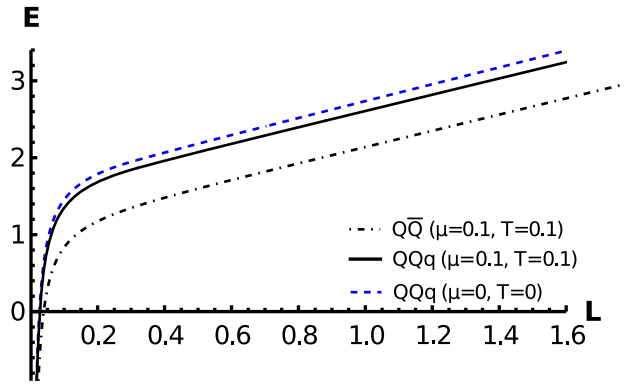

FIG. 5. E as a function of L for QQq and $\mathrm{Q\bar{Q}}$. The solid black and dashed blue lines correspond to the variations of E as a function of L for QQq at $\mu=0.1$ GeV, $T=0.1$ GeV, and $\mu=0$ GeV, $T=0$ GeV, respectively. The dash-dotted black line represents the variations for $\mathrm{Q\bar{Q}}$ at $\mu=0.1$ GeV, $T=0.1$ GeV. The unit of E is GeV, and L is fm.

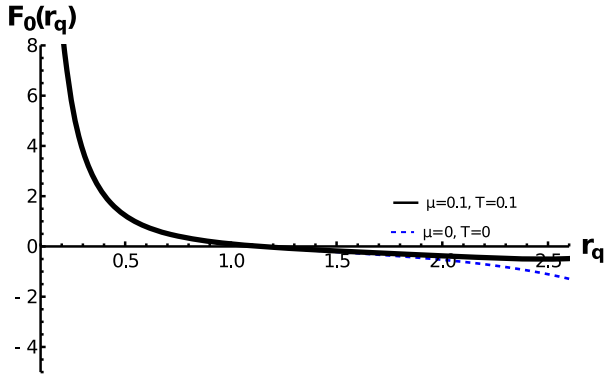

FIG. 6. The force balance equations as functions of r_q. The solid black and dashed blue lines correspond to $\mu = 0.1$ GeV, $T = 0.1$ GeV, and $\mu = 0$ GeV, $T = 0$ GeV, respectively. r_q is the position of light quark. The unit of r_q is GeV^{-1}.

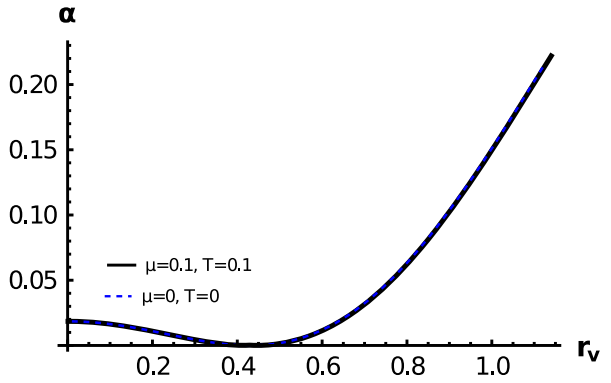

FIG. 7. α as a function of r_v for QQq in small separate distance. The solid black and dashed blue lines correspond to $\mu = 0.1$ GeV, $T = 0.1$ GeV, and $\mu = 0$ GeV, $T = 0$ GeV, respectively. The unit of r_v is GeV^{-1}.

and compare with that of doubly heavy baryon under the same external conditions. While the overall behavior of potential energy also follows a Cornell-like potential, $Q\bar{Q}$ has a lower potential energy at equal separate distances. Besides, it is shown that the presence of temperature and chemical potential will decrease the linear part of the Cornell-like potential.

In addition, despite μ having been considered in the model, the potential energy is still the Coulomb potential in small L (the first configuration) and linear potential in intermediate and large L (the later two configurations). Theoretically, L can grow to infinity as r_v increases if no string melting occurs.

When $T = 0.1$ GeV, $\mu = 0.1$ GeV, all string configurations exist. According to Eq. (20), the force balance equation of the light quark $F_0(r_q)$ is plotted in Fig. 6. At the same time, we further gain understanding of the change for string structure by observing the variation for angle α. For the three configurations mentioned above, we solve the force balance equations at the baryon vertex to obtain a plot of the variation of angle α with r_v for the three configurations as shown in Figs. 7–9, respectively. At a small separate distance, α first decreases and then increases as r_v increases. At an intermediate separate distance, α slowly decreases from $\alpha \approx 0.221$ to zero as r_v increases. At a large separate distance, as r_v increases, angle α becomes negative and continues to decrease monotonically. Besides, it is shown that the temperature and chemical potential have minimal effect at small separate distances.

B. String breaking

In this subsection, we fixed $T = 0.1$ GeV and set $\mu = 0$, 0.1, and 0.22 GeV, respectively. As is well known, due to the restriction of energy, string breaking will occur at a critical length when the separation distance L increases. At this point, the energy of the string reaches a critical level where it can no longer remain stable. It breaks apart and

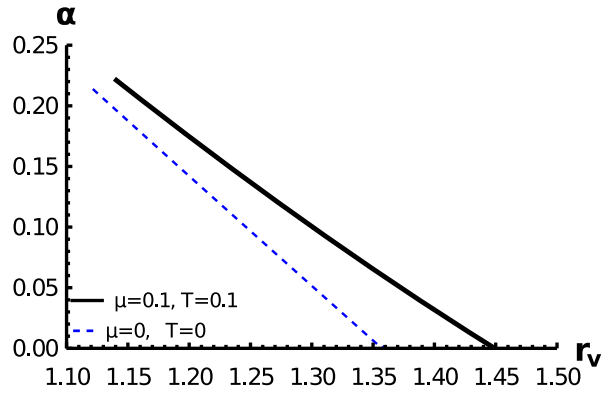

FIG. 8. α as a function of r_v for QQq in intermediate separate distance. The solid black and dashed blue lines correspond to $\mu = 0.1$ GeV, $T = 0.1$ GeV, and $\mu = 0$ GeV, $T = 0$ GeV, respectively. The unit of r_v is GeV^{-1}.

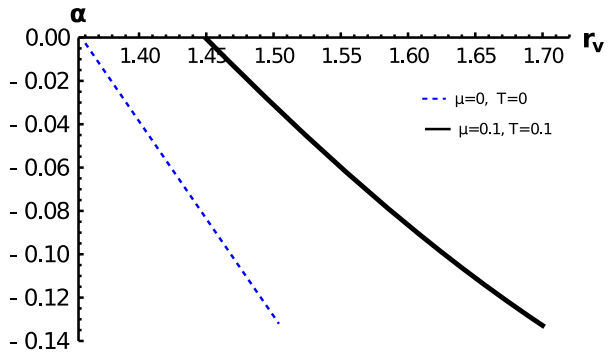

FIG. 9. α as a function of r_v for QQq in large separate distance. The solid black and dashed blue lines correspond to $\mu = 0.1$ GeV, $T = 0.1$ GeV, and $\mu = 0$ GeV, $T = 0$ GeV, respectively. The unit of r_v is GeV^{-1}.

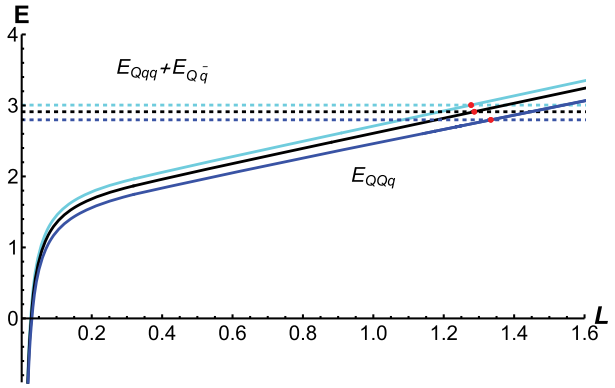

FIG. 10. E as a function of L. The cyan line, the black line, and the blue line represent $\mu = 0$, 0.1, and 0.22 GeV, respectively. T remains 0.1 GeV. The dashed line shows the potential energy after decay. The unit of E is GeV, and L is fm.

becomes two different string structures. In our paper, we are interested in the decay mode of $QQq \to Qqq + Q\bar{q}$. The renormalized total energy is

$$E_{Qqq} + E_{Q\bar{q}} = \mathbf{g}\left(2\int_{r_v}^{r_q}\frac{e^{sr^2}}{r^2}dr + \int_0^{r_q}\left(\frac{e^{sr^2}}{r^2} - \frac{1}{r^2}\right) - \frac{1}{r_q} + \int_0^{r_v}\left(\frac{e^{sr^2}}{r^2} - \frac{1}{r^2}\right) - \frac{1}{r_v} + 3k\frac{e^{-2sr_v^2}\sqrt{f(r_v)}}{r_v} + 3n\frac{e^{\frac{1}{2}sr_q^2}}{r_q}\sqrt{f(r_q)}\right) + 2c. \quad (34)$$

Expressions for the breaking distances give characteristic scales when string breaking takes place [14,16]. The potential energy and the schematic diagram of string breaking are presented in Figs. 10 and 11, respectively. As can be seen from Fig. 10, with the increase of μ, the energy of the breaking point decreases, and the separate

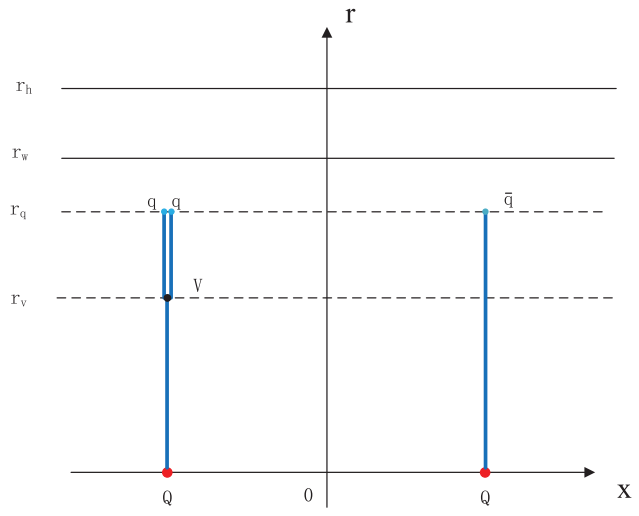

FIG. 11. A schematic diagram of $Qqq + Q\bar{q}$.

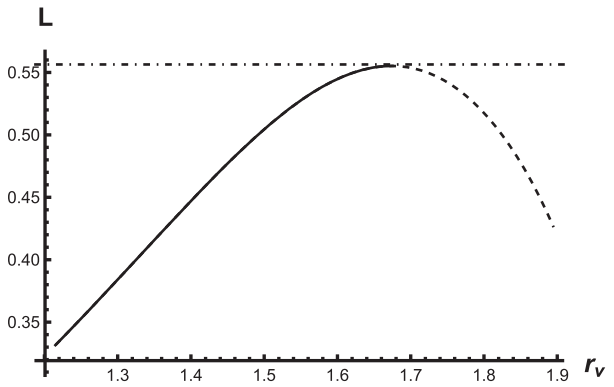

FIG. 12. L as a function of r_v at $\mu = 0.35$ GeV and $T = 0.1$ GeV. The part indicated by the dashed line means that the string has melted and has no physical significance. The dotted lines represent the maximum value of potential energy. The unit of L is fm, and r_v is GeV^{-1}.

distance increases. It means the QQq configuration is more stable at small chemical potential.

C. String melting

When string melting occurs, the diagram of $L - r_v$ is shown in Fig. 12. To study the μ-dependent of string melting, we fixed $T = 0.1$ GeV and μ to 0.3, 0.35, and 0.4 GeV, respectively. The results of $E - L$ at different chemical potentials are presented in Fig. 13. As the string of $Q\bar{Q}$ also melts under $T = 0.1$ GeV and $\mu = 0.35$ GeV, we compare the potential of QQq and $Q\bar{Q}$ in Fig. 14. When μ is fixed to 0.05 GeV, we plot E as a function of L at different T in Fig. 15. The correspondence between E and L is almost independent of temperature until the string melts. Furthermore, we study the melt of QQq at the different temperatures and chemical potentials in Fig. 16. It is found that the influence of temperature is larger than chemical potential.

As can be seen from Fig. 13, with the increase of μ, the melting point moves to the lower left. This means that

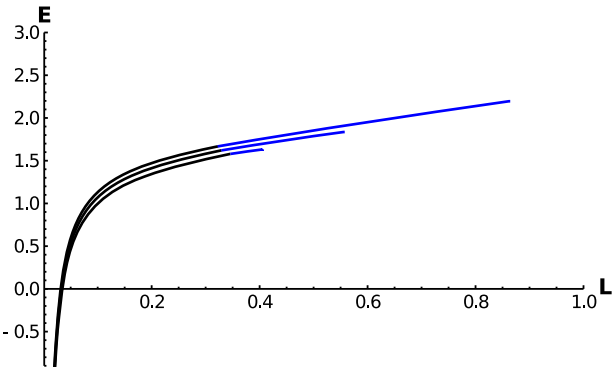

FIG. 13. E as a function of L when T is fixed to 0.1 GeV. From top to bottom, μ is 0.3, 0.35, and 0.4 GeV, respectively. The unit of E is GeV, and L is fm.

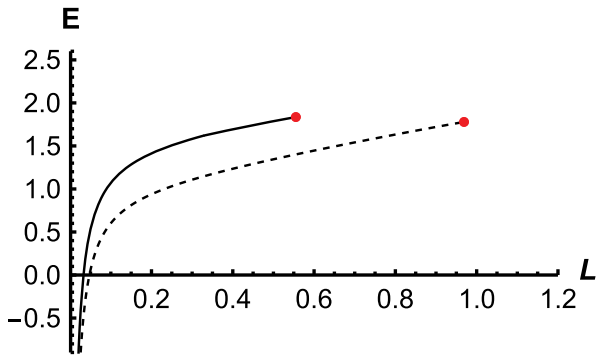

FIG. 14. E as a function of L at $T = 0.1$ GeV and $\mu = 0.35$ GeV. The solid line and the dashed line correspond to QQq and $Q\bar{Q}$, respectively. The unit of E is GeV, and L is fm.

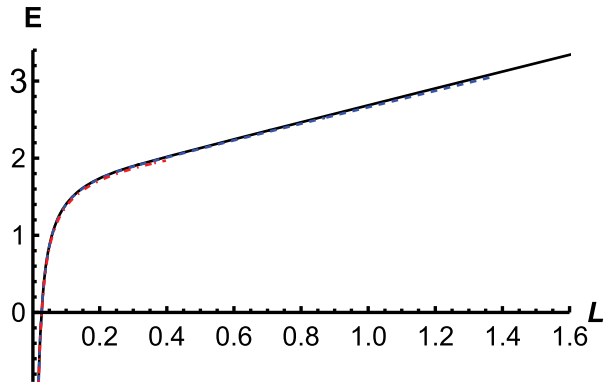

FIG. 15. E as a function of L at different T when $\mu = 0.05$ GeV. The black solid line, the blue dashed line, and the red dot-dashed line correspond to $T = 0.05$ GeV, $T = 0.1$ GeV, and $T = 0.146$ GeV, respectively. The unit of E is GeV, and L is fm.

string melting is more likely to occur at higher chemical potentials. From Figs. 4 and 12, we can compare the differences of QQq between small chemical potential and large chemical potential. When the string melting condition is not satisfied, the separation distance between quarks (L) increases monotonically as the r_v increase. Once string melting condition is satisfied, L first increases and then decreases as r_v increases. However, the decreasing part of the L indicated by a dashed line is unphysical.

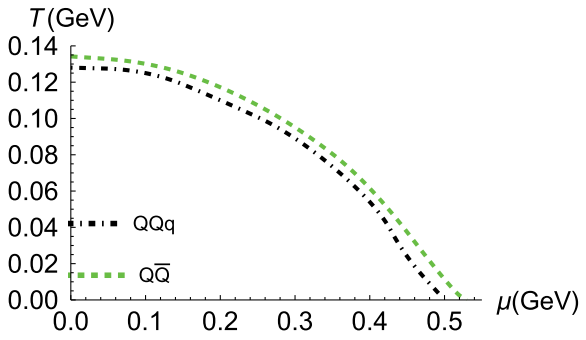

FIG. 17. The melting diagram of doubly heavy baryon and quark-antiquark pairs in the $T - \mu$ plane in units GeV.

Furthermore, the melting diagram can be drawn in a $T - \mu$ plane if enough data of (μ, T) points are found. The comparison with $Q\bar{Q}$ [57] is also shown in Fig. 17. From the diagram above, the melting line of QQq is lower than quark-antiquark pairs. In other words, we can infer that the quark-antiquark pair is more stable than the doubly heavy baryon.

D. Two critical chemical potentials

In this section, we discuss the relation between possible string configurations and μ. It is found that the presence of temperature and chemical potential can make QQq unstable. By setting T close to zero, we can determine the chemical potential at which Eq. (20) has no solutions. We have found the critical value of the chemical potential to be 0.633 GeV at $T = 0.001$ GeV, which means the first configurations cannot exist. The result is presented in Fig. 18. At the same temperature, the QQq state melts at intermediate separation distances for $\mu = 0.498$ GeV. The string will melt at the second configuration. We can conclude that QQq has three configurations at small chemical potential and the temperature close to zero. When $\mu > 0.498$ GeV, only two configurations can exist.

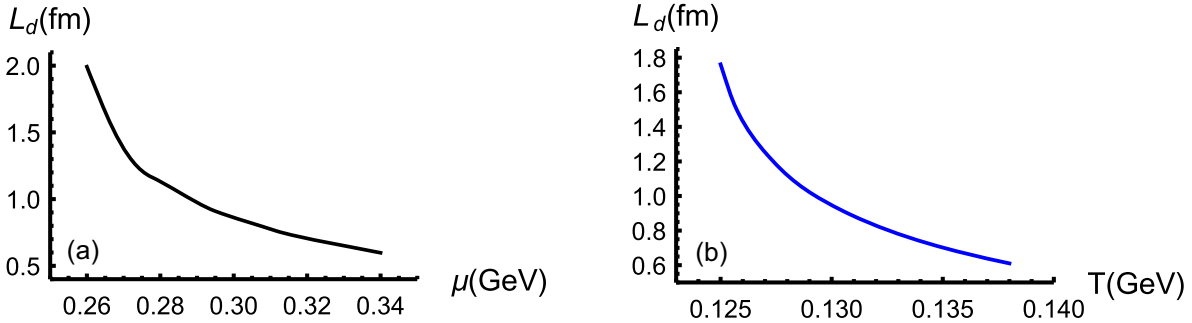

FIG. 16. (a) The screening distance L_d as a function of μ at $T = 0.1$ GeV. (b) The screening distance L_d as a function of T at $\mu = 0.1$ GeV.

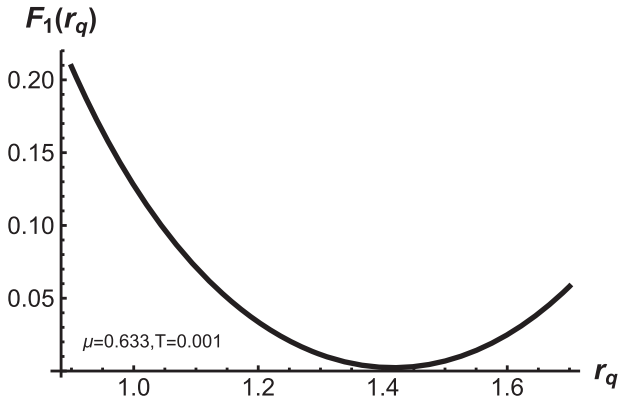

FIG. 18. The force balance equations as a function of r_q in the first configuration. r_q is the position of light quark, $\mu_{c2} = 0.633$ GeV and $T = 0.001$ GeV. The unit of r_q is GeV^{-1}.

Beyond 0.633 GeV, even the first configuration of QQq cannot exist.

IV. SUMMARY AND CONCLUSIONS

In this paper, we mainly discussed the potential energy, the string breaking, and QQq melting at finite temperature and chemical potential through a five-dimensional effective string model. Even with the introduction of temperature and chemical potential, the overall potential energy behavior still exhibits a Coulomb potential at small separate distances, becoming a linear potential at large separate distances. As the chemical potential increases, string breaking occurs at a larger separate distance and lower potential energy in the decay mode $\mathrm{QQq} \to \mathrm{Qqq} + \mathrm{Q\bar{q}}$. We discussed the string melting of QQq at a fixed temperature and chemical potential, respectively, and compared them with $\mathrm{Q\bar{Q}}$. It is found that the potential energy of QQq and $\mathrm{Q\bar{Q}}$ is very close when the string melts. In both cases, QQq melts at a smaller separate distance. Finally, we draw the melting diagram of QQq and $\mathrm{Q\bar{Q}}$ in the $T - \mu$ plane. The melting line of QQq is below that of $\mathrm{Q\bar{Q}}$, which indicates that QQq is less stable than $\mathrm{Q\bar{Q}}$.

ACKNOWLEDGMENTS

This work is supported by the Natural Science Foundation of Hunan Province of China under Grant No. 2022JJ40344, the Research Foundation of Education Bureau of Hunan Province, China (Grant No. 21B0402) and the National Natural Science Foundation of China (Grant No. 12175100).

[1] C. B. Lang and C. Rebbi, Phys. Lett. **115B**, 137 (1982).
[2] J. Hoek, Z. Phys. C **35**, 369 (1987).
[3] C. Michael and S. J. Perantonis, J. Phys. G **18**, 1725 (1992).
[4] T. T. Takahashi, H. Suganuma, Y. Nemoto, and H. Matsufuru, Phys. Rev. D **65**, 114509 (2002).
[5] Y. Aoki, Z. Fodor, S. D. Katz, and K. K. Szabo, J. High Energy Phys. 01 (2006) 089.
[6] C. Ratti, M. A. Thaler, and W. Weise, Phys. Rev. D **73**, 014019 (2006).
[7] P. Bicudo, M. Cardoso, and O. Oliveira, Phys. Rev. D **77**, 091504 (2008).
[8] M. Lüscher, J. High Energy Phys. 08 (2010) 071; 03 (2014) 92(E).
[9] P. Hasenfratz and F. Karsch, Phys. Lett. **125B**, 308 (1983).
[10] Z. Fodor and S. D. Katz, Phys. Lett. B **534**, 87 (2002).
[11] S. Muroya, A. Nakamura, C. Nonaka, and T. Takaishi, Prog. Theor. Phys. **110**, 615 (2003).
[12] N. Brambilla, Systems of two heavy quarks with effective field theories, in *Continuous Advances in QCD 2006* (World Scientific, Singapore, 2007).
[13] J. Ghiglieri, arXiv:1201.2920.
[14] O. Andreev, Phys. Rev. D **101**, 106003 (2020).
[15] O. Andreev, Phys. Rev. D **104**, 026005 (2021).
[16] O. Andreev, Phys. Lett. B **804**, 135406 (2020).
[17] E. Eichten, K. Gottfried, T. Kinoshita, K. D. Lane, and T. M. Yan, Phys. Rev. D **17**, 3090 (1978); **21**, 313(E) (1980).
[18] E. Eichten, K. Gottfried, T. Kinoshita, K. D. Lane, and T. M. Yan, Phys. Rev. D **21**, 203 (1980).
[19] O. Andreev, J. High Energy Phys. 05 (2021) 173.
[20] Y. Sumino, Phys. Lett. B **595**, 387 (2004).
[21] O. Andreev and V. I. Zakharov, Phys. Lett. B **645**, 437 (2007).
[22] I. I. Balitsky, Nucl. Phys. **B254**, 166 (1985).
[23] P. de Forcrand and O. Jahn, Nucl. Phys. **A755**, 475 (2005).
[24] O. Andreev and V. I. Zakharov, J. High Energy Phys. 04 (2007) 100.
[25] S. He, M. Huang, and Q.-S. Yan, Prog. Theor. Phys. Suppl. **186**, 504 (2010).
[26] P. Colangelo, F. Giannuzzi, and S. Nicotri, Phys. Rev. D **83**, 035015 (2011).
[27] O. DeWolfe, S. S. Gubser, and C. Rosen, Phys. Rev. D **83**, 086005 (2011).
[28] D. Li, S. He, M. Huang, and Q. S. Yan, J. High Energy Phys. 09 (2011) 041.
[29] K. B. Fadafan, Eur. Phys. J. C **71**, 1799 (2011).
[30] K. B. Fadafan and E. Azimfard, Nucl. Phys. **B863**, 347 (2012).
[31] R. G. Cai, S. He, and D. Li, J. High Energy Phys. 03 (2012) 033.
[32] D. Li, M. Huang, and Q. S. Yan, Eur. Phys. J. C **73**, 2615 (2013).
[33] Z. Fang, S. He, and D. Li, Nucl. Phys. **B907**, 187 (2016).

[34] Y. Yang and P. H. Yuan, J. High Energy Phys. 12 (2015) 161.
[35] Z.-q. Zhang, D.-f. Hou, and G. Chen, Nucl. Phys. **A960**, 1 (2017).
[36] C. Ewerz, O. Kaczmarek, and A. Samberg, J. High Energy Phys. 03 (2018) 088.
[37] X. Chen, S. Q. Feng, Y. F. Shi, and Y. Zhong, Phys. Rev. D **97**, 066015 (2018).
[38] I. Aref'eva and K. Rannu, J. High Energy Phys. 05 (2018) 206.
[39] X. Chen, D. Li, and M. Huang, Chin. Phys. C **43**, 023105 (2019).
[40] H. Bohra, D. Dudal, A. Hajilou, and S. Mahapatra, Phys. Lett. B **801**, 135184 (2020).
[41] X. Chen, D. Li, D. Hou, and M. Huang, J. High Energy Phys. 03 (2020) 073.
[42] J. Zhou, X. Chen, Y. Q. Zhao, and J. Ping, Phys. Rev. D **102**, 086020 (2020).
[43] J. Zhou, X. Chen, Y. Q. Zhao, and J. Ping, Phys. Rev. D **102**, 126029 (2021).
[44] X. Chen, L. Zhang, D. Li, D. Hou, and M. Huang, J. High Energy Phys. 07 (2021) 132.
[45] X. Chen, L. Zhang, and D. Hou, Chin. Phys. C **46**, 073101 (2022).
[46] D. J. Gross and H. Ooguri, Phys. Rev. D **58**, 106002 (1998).
[47] J. M. Maldacena, Adv. Theor. Math. Phys. **2**, 231 (1998).
[48] J. M. Maldacena, Phys. Rev. Lett. **80**, 4859 (1998).
[49] S. J. Rey and J. T. Yee, Eur. Phys. J. C **22**, 379 (2001).
[50] S. J. Rey, S. Theisen, and J. T. Yee, Nucl. Phys. **B527**, 171 (1998).
[51] E. Witten, J. High Energy Phys. 07 (1998) 006.
[52] O. Andreev, Phys. Lett. B **756**, 6 (2016).
[53] O. Andreev, Phys. Rev. D **93**, 105014 (2016).
[54] O. Andreev and V. I. Zakharov, Phys. Rev. D **74**, 025023 (2006).
[55] O. Andreev, Phys. Rev. D **86**, 065013 (2012).
[56] Xun Chen, Bo Yu, Peng-Cheng Chu, and Xiao-hua Li, Chin. Phys. C **46**, 073102 (2022).
[57] J. J. Jiang, Y. Z. Xiao, J. Qin, X. Li, and X. Chen, Chin. Phys. C **47**, 013106 (2023).